# Quantum Chemical Investigation of Ethylene Insertion into the Cr−$CH_3$ Bond in $CrCl(H_2O)CH_3^+$ as a Model of Homogeneous Ethylene Polymerization

Vidar R. Jensen* and Knut J. Børve

*Department of Chemistry, University of Bergen, Allégaten 41, N-5007 Bergen, Norway*

*Received November 1, 1996*[⊗]

Direct ethylene insertion for the title Cr(III) system is shown to be a feasible reaction, which suggests that polymerization with the recently developed homogeneous Cr(III)-based catalysts follows this mechanism. The present results parallel to a large extent those reported earlier for models of Ti(IV)- and Zr(IV)-based catalysts. However, the transition state of insertion is located later during insertion than what has been reported for the group 4 catalysts, and the calculated activation energy is slightly higher. The catalyzing abilities of chromium(III) are discussed and related to the metal electron configuration and the possibility of the d orbitals participating in bond formation. A number of quantum chemical methods and basis sets are compared with respect to predictions for the present reaction. Second-order perturbation theory, size-consistent configuration interaction, as well as gradient-corrected density functional theory methods, together with basis sets of double-$\zeta$ plus polarization quality, provide feasible and adequate descriptions of the reaction at hand.



## 1. Introduction

Chromium holds a prominent position among the metals that polymerize ethylene, with the Phillips[1] and Union Carbide[2,3] silica-supported catalysts being of large commercial importance. An intense effort has been put into identifying the active catalytic species and likely mechanisms for the propagation, but still basic properties of the active species, such as oxidation state, are being discussed, see *e.g.* ref 4. Similar problems have been encountered also for other supported polymerization catalysts, see *e.g.* refs 5 and 6, but the study of chromium-based catalysts has been particularly hampered by a lack of active and well-defined homogeneous counterparts to the supported catalysts. Except for the half-sandwich Cr(III) systems of Theopold *et al.*[7−10] and the bis(imido)Cr(VI) alkyl cations of Gibson *et al.*,[11] such examples remain rare. In contrast, homogeneous group 4 catalysts for olefin polymerization date back to the original discovery by Ziegler;[12] they are generally well-defined and several active species have been identified.[13−15] The identified structures, or models of such, have in turn been used in molecular modeling of the propagation[16−31] and termination[24,28−31] process, thus contributing further to the understanding of the function of these catalysts. To our knowledge, only one quantum chemical study of polymerization with a chromium-based system has so far been reported.[32]

In recent years, Theopold and co-workers[7−10] have published a series of studies of ethylene polymerizations

[⊗] Abstract published in *Advance ACS Abstracts,* May 1, 1997.

(1) Phillips Petroleum Company. U.S. Patent 2825721, Jan 1953.
(2) Garrick, W. L.; Turbett, R. J.; Karol, F. J.; Karapinka, G. L.; Fox, A. S.; Johnson, R. N. *J. Polym. Sci., Part A-1* **1972**, *10*, 2609.
(3) Karol, F. J.; Karapinka, G. L.; Wu, C.; Dow, A. W.; Johnson, R. N.; Garrick, W. L. *J. Polym. Sci., Part A-1* **1972**, *10*, 2621.
(4) Feher, F. J.; Blanski, R. L. *J. Chem. Soc., Chem. Commun.* **1990**, 1614.
(5) Ystenes, M. *J. Catal.* **1991**, *129*, 383.
(6) Chien, J. C. W. in *Catalysis in Polymer Synthesis*; Vandenberg, E. J., Salamone, J. C., Eds.; ACS Symposium Series 496; American Chemical Society: Washington, DC, 1992; Chapter 2.
(7) Thomas, B. J.; Theopold, K. H. *J. Am. Chem. Soc.* **1988**, *110*, 5902.
(8) Thomas, B. J.; Noh, S. K.; Schulte, G. K.; Sendlinger, S. C.; Theopold, K. H. *J. Am. Chem. Soc.* **1991**, *113*, 893.
(9) Theopold, K. H.; Heintz, R. A.; Noh, S. K.; Thomas, B. J. In *Homogeneous Transition Metal Catalyzed Reactions*; Moser, W. R.; Slocum, D. W., Eds.; Advances in Chemistry Series 230; American Chemical Society: Washington, DC, 1992; Vol. 103, p 591.
(10) Bhandari, G.; Kim, Y.; McFarland, J. M.; Rheingold, A. L.; Theopold, K. H. *Organometallics* **1995**, *14*, 738.
(11) Coles, M. P.; Dalby, C. I.; Gibson, V. C.; Clegg, W.; Elsegood, M. R. J. *J. Chem. Soc., Chem. Commun.* **1995**, 1709.
(12) Ziegler, K. Belg. Patent 533362, Nov 1953.
(13) Eisch, J. J.; Caldwell, K. R.; Werner, S.; Krüger, C. *Organometallics* **1991**, *10*, 3417.
(14) Alelyunas, Y. W.; Jordan, R. F.; Echols, S. F.; Borkowsky, S. L.; Bradley, P. K. *Organometallics* **1991**, *10*, 1406.
(15) Yang, X.; Stern, C. L.; Marks, T. J. *J. Am. Chem. Soc.* **1991**, *113*, 3623.
(16) Fujimoto, H.; Yamasaki, T.; Mizutani, H.; Koga, N. *J. Am. Chem. Soc.* **1985**, *107*, 6157.
(17) Jolly, C.; Marynick, D. S. *J. Am. Chem. Soc.* **1989**, *111*, 7968.
(18) Kawamura-Kuribayashi, H.; Koga, N.; Morokuma, K. *J. Am. Chem. Soc.* **1992**, *114*, 2359.
(19) Kawamura-Kuribayashi, H.; Koga, N.; Morokuma, K. *J. Am. Chem. Soc.* **1992**, *114*, 8687.
(20) Castonguay, L. A.; Rappé, A. K. *J. Am. Chem. Soc.* **1992**, *114*, 5832.
(21) Axe, F. U.; Coffin, J. M. *J. Phys. Chem.* **1994**, *98*, 2567.
(22) Weiss, H.; Ehrig, M.; Ahlrichs, R. *J. Am. Chem. Soc.* **1994**, *116*, 4919.
(23) Meier, R. J.; van Doremaele, G. H. J.; Iarlori, S.; Buda, F. *J. Am. Chem. Soc.* **1994**, *116*, 7274.
(24) Woo, T. K.; Fan, L.; Ziegler, T. *Organometallics* **1994**, *13*, 2252.
(25) Bierwagen, E. P.; Bercaw, J. E.; Goddard, W. A., III. *J. Am. Chem. Soc.* **1994**, *116*, 1481.
(26) Jensen, V. R.; Børve, K. J.; Ystenes, M. *J. Am. Chem. Soc.* **1995**, *117*, 4109.
(27) Fan, L.; Harrison, D.; Woo, T. K.; Ziegler, T. *Organometallics* **1995**, *14*, 2018.
(28) Yoshida, T.; Koga, N.; Morokuma, K. *Organometallics* **1995**, *14*, 746.
(29) Lohrenz, J. C. W.; Woo, T. K.; Ziegler, T. *J. Am. Chem. Soc.* **1995**, *117*, 12793.
(30) Margl, P.; Lohrenz, J. C. W.; Ziegler, T.; Blöchl, P. E. *J. Am. Chem. Soc.* **1996**, *118*, 4434.
(31) Støvneng, J. A.; Rytter, E. *J. Organomet. Chem.* **1996**, *519*, 277.
(32) Armstrong, D. R.; Fortune, R.; Perkins, P. G. *J. Catal.* **1976**, *42*, 435.

S0276-7333(96)00930-2 CCC: $14.00 

**Table 1. Basis Set Contractions Used for Calculating Ethylene Insertion in $CrCl(H_2O)CH_3^+$ [a]**

| basis | Cr | Cl | O, C | H |
|---|---|---|---|---|
| A | (14s11p6d3f)/[5s4p3d1f] | (12s10p1d)/[4s4p1d] | (9s5p1d)/[3s2p1d] | (5s1p)/[3s1p] |
| B | (14s11p6d)/[10s8p3d] | (12s8p1d)/[6s4p1d] | (10s5p1d)/[3s2p1d] | (4s)/[2s] |
| C | (14s11p6d3f)/[10s8p3d1f] | (12s8p1d)/[6s4p1d] | (10s5p1d)/[3s2p1d] | (4s1p)/[2s1p] |
| D | (14s11p6d6f)/[8s6p4d2f] | (13s10p2d)/[7s6p2d] | (11s7p2d)/[6s4p2d] | (6s2p)/[4s2p] |

[a] Sets A are generally contracted,[41,42] while the others are segmented.

using homogeneous chromium-based catalysts. The catalytically most active structures are cationic, neutral, or anionic four-coordinate chromium(III) alkyls, one of the ligands always being pentamethylcyclopentadienyl, Cp*. The charge on the chromium alkyl complex is determined by the number of additional covalent ligands (alkyl groups). Neutral catalysts of this kind, thus, have two alkyl groups and the fourth ligand is a relatively weakly bound donor, tetrahydrofuran (THF). Catalytically active cationic chromium alkyls have only a single alkyl group and two THF ligands, as exemplified by $[CrCp^*(THF)_2CH_3]^+$ $BPh_4^-$.[7] The fact that all of the active catalyst precursors of this kind have been been based on Cr(III) alkyls, despite attempts to obtain the corresponding active chromium(II) species[9,33] suggests that the active oxidation state is actually +III. However, no conclusive evidence as to the active oxidation state has been put forward so far.

Among the catalysts presented by the group of Theopold, the cationic $CrCp^*(THF)_2CH_3^+$ is of particular interest because of the apparent similarity to cations reported to constitute the active species in group 4 metallocene catalysts.[1315] In a solution of dichloromethane (room temperature and 1.0−1.5 atm) the activity of the cationic chromium(III) alkyl reached a turnover frequency of ∼0.7 $s^{-1}$, with reduced activity upon addition of THF. Theopold *et al.*[9] proposed that this reduction is due to the presence of a dissociation equilibrium for THF and that the active species itself contains only one THF ligand, leaving a coordination site open for the binding of ethylene.

In the present paper, we will investigate ethylene insertion for a model of the cationic mono-THF system, $CrCp^*(THF)CH_3^+$, which Theopold *et al.* proposed to be active. The main reason for studying the cation is the possibility of comparing the results with the previous theoretical studies of corresponding cations of group 4 transition metals. To gain experience with the quantum chemical description of alkene insertion using chromium(III), it is desirable to employ a range of different methods. In turn, the required number of quantum chemical calculations calls for the use of a simplified model for the real catalyst. Here, Cp* is modeled by Cl and THF by $H_2O$, thus obtaining $CrCl(H_2O)CH_3^+$. Cl has frequently been used as a model for Cp in theoretical studies of polymerizations using group 4 transition metals,[16−18,20−22,26] which thus provides us with relevant data for comparison with the present chlorine-containing model. The main goal of the present study is to obtain a qualitative insight into the function of chromium(III) as an ethylene polymerization catalyst and, in particular, to compare it with titanium(IV).

From the outset, it is clear that difficulties due to near-degeneracy can be expected from a first-row transition metal system,[34] at least when the system is not of the formal $d^0$ character. Thus, the methods employed should include a configuration interaction (CI) method that is relatively stable toward these effects. We have chosen the modified coupled-pair functional (MCPF) method[35] for these calculations. In future calculations on chromium-based catalysis, it will be desirable to use larger, more realistic models. Thus, we also include results from computationally less demanding methods, like Hartree−Fock (HF), second-order perturbation theory (MP2), the local spin density approximation (LSDA), as well as two gradient-corrected density functional theory (DFTG) methods.

While the present work was in progress, Gibson *et al.*[11] reported a dibenzyl chromium(VI) compound, $Cr(NR)_2(CH_2R')_2$ (R = $Bu^t$, R′ = Ph) to be a surprisingly active catalyst for the polymerization of ethylene. After treatment with $[Ph_3C][B(C_6F_5)_4]$ in dichloromethane, a monobenzyl cationic complex is reportedly obtained, of which the latter appears to be the active species. The isolobal relationship between this monobenzyl cation and the highly active alkyl cations present in group 4 metallocene catalysts[13−15] makes further studies of the imidochromium(VI) systems seem very promising. Thus, in our lab, we are currently performing a quantum chemical investigation of ethylene insertion using bis(imido)chromium(VI) alkyl cations.

## 2. Computational Details

The calculations were performed on local DEC workstations at the University of Bergen and on IBM workstations at the National Supercomputing Center at the University of Oslo.

**2.1. Basis Sets.** The calculations were performed using spherical harmonics bases, except for geometry optimizations at the HF level for which Cartesian bases were used. Four different basis sets, labeled A, B, C, and D, were used in the present work. The contractions are given in Table 1.

**2.1.1. Geometry Optimizations.** All geometry optimizations were performed using the B sets described as follows. For chromium, a Wachters primitive basis[36] contracted to [10s8p3d] with the standard modifications as implemented in GAMESS[37] was used. All ligand atoms were described by valence double-ζ sets based on atomic calculations by Huzinaga[38,39] and with contraction schemes from Dunning *et al.*[40] A polarization function was added for all heavy atoms: $\alpha_d$ = 0.75 for chlorine and carbon and $\alpha_d$ = 0.85 for oxygen. A scale factor of 1.2 (1.15) was applied for the inner (outer) exponents of hydrogen.

(33) Heintz, R. A.; Ostrander, R. L.; Rheingold, A. L.; Theopold, K. H. *J. Am. Chem. Soc.* **1994**, *116*, 11387.

(34) Siegbahn, P. E. M.; Svensson, M. *Chem. Phys. Lett.* **1993**, *216*, 147.

(35) Chong, D. P.; Langhoff, S. R. *J. Chem. Phys.* **1986**, *84*, 5606.

(36) Wachters, A. J. H. *J. Chem. Phys.* **1970**, *52*, 1033.

(37) Schmidt, M. W.; Baldridge, K. K.; Boatz, J. A.; Elbert, S. T.; Gordon, M. S.; Jensen, J. H.; Koseki, S.; Matsunaga, N.; Nguyen, K. A.; Su, S. J.; Windus, T. L.; Dupuis, M.; Montgomery, J. A. *J. Comput. Chem.* **1993**, *14*, 1347.

(38) Huzinaga, S. *J. Chem. Phys.* **1965**, *42*, 1293.

(39) Huzinaga, S. Approximate atomic functions II. Report to the Department of Chemistry; University of Alberta: Alberta, Canada, 1971.

(40) Dunning, T. H.; Hay, P. J. in *Methods of Electronic Structure Theory*; Schaefer, H. F., Ed.; Plenum Press: New York, 1977; Chapter 1.

**2.1.2. Energy Evaluations.** The A sets follow a general contraction scheme[41,42] and are essentially of double-ζ plus polarization quality. For Cr, Wachters' primitive basis[36] was extended by adding one diffuse d function ($\alpha_d = 0.0912$), two p functions ($\alpha_p = 0.181\ 01, 0.057\ 92$), and three f functions ($\alpha_f = 2.731\ 320\ 3, 0.979514, 0.4194397$). For chlorine, the Huzinaga primitive basis[39] was augmented by one diffuse p function ($\alpha_p = 0.044$) and one d function ($\alpha_d = 0.55$). For carbon, the Huzinaga primitive (9s5p) basis[38] was extended with one d function ($\alpha_d = 0.63$). Oxygen was described by the primitive (9s5p) basis of van Duijneveldt,[43] augmented by one d function ($\alpha_d = 1.33$). Hydrogen was described by the Huzinaga primitive (5s) basis,[38] augmented by one p function ($\alpha_p = 0.8$).

The C sets differ from B only for Cr and H. For chromium, a primitive (3f) set contracted to [1f] was added to the B set, while a p function ($\alpha_p = 1.0$) was added to the B set for hydrogen.

Our largest sets (D) are essentially valence triple-ζ with double-ζ polarization as well as diffuse s and p functions, added in an even tempered manner on all ligands. For chromium, Wachters' primitive basis[36] was used with the 4p exponents multiplied by 1.5 and with a diffuse d exponent ($\alpha_d = 0.0912$) added. The contraction of (14s11p6d) followed Wachters' scheme 3. This chromium basis was augmented by a primitive (6f) basis[44] generally contracted to [2f]. Chlorine was described by a Huzinaga primitive (12s9p) basis[39] contracted according to McLean and Chandler's chloride scheme[45] to [6s5p]. Diffuse s and p functions and two d functions ($\alpha_d = 1.299, 0.433$) were added. For oxygen and carbon, a Huzinaga primitive (10s6p) basis[38] contracted to [5s3p][46] and augmented by two d functions ($\alpha_d = 1.5, 0.5$ for oxygen and $\alpha_d = 1.299, 0.433$ for carbon) was used. Diffuse s and p functions were added. Hydrogen was described by a scaled (factor 1.49) Huzinaga primitive (5s) set[38] contracted to [3s].[46] One diffuse s function was added along with two p functions ($\alpha_p = 1.7, 0.6$).

**2.2. Methods.** Restricted determinants were used to form wave functions in all calculations on closed shell systems. In *ab initio* calculations on open shell systems, a restricted open shell formulation was used. Unrestricted determinants were used to form wave functions in all density functional theory (DFT) calculations on open shell systems. In all DFT calculations, the density was evaluated using a grid with 75 radial shells per atom and 302 angular points per shell.

**2.2.1. Geometry Optimizations.** Geometries were optimized using three different methods: Hartree−Fock (HF), the local spin density approximation (LSDA) involving Slater exchange and the correlation functional V from the paper by Vosko *et al.*[47] and finally with gradient-corrected density functional theory (BPW91) using Becke's 1988 exchange functional[48] along with Perdew and Wang's 1991 correlation functional.[49]

Stationary points were fully optimized within the respective symmetries ($C_1$ for the model catalyst) by means of analytical gradient techniques. The stationary points were characterized by checking the curvature of the potential energy surface (PES). The corresponding Hessian matrices were calculated analytically. Frequencies were obtained within the harmonic approximation.

Geometry optimizations at the HF level were performed using the GAMESS set of programs,[37] and geometries were converged to a maximum gradient below $10^{-4}$ hartree/bohr. Optimizations at the two correlated levels were performed by means of the Gaussian 94 set of programs.[50] Geometries were converged to a maximum gradient and displacement of $4.5 \times 10^{-4}$ hartree/bohr and $1.8 \times 10^{-3}$ bohr, respectively.

**2.2.2. Energy Evaluations.** In addition to the methods used for geometry optimization (see above), energies are reported for methods based on hybrid DFT, perturbation theory, and, finally, configuration interaction (CI) theory. The hybrid DFT method was Becke's three-parameter functional (B3LYP).[51] This functional includes HF and Slater exchange as well as Becke's 1988 exchange functional correction.[48] Correlation is provided both by the expression according to Lee *et al.*[52] and the local correlation functional by Vosko *et al.*[47] Perturbation theory was applied in terms of second-order Møller−Plesset theory (MP2),[53] with all valence electrons correlated. All MP2 and DFT calculations were performed using the Gaussian 94 set of programs.[50] The CI method used was the modified coupled-pair functional (MCPF) approximation,[35] which is a size-consistent, single-reference state method. The zero-order wave functions were defined at the HF level. All valence electrons except chlorine 3s were correlated, and the core orbitals as well as the 3s on chlorine were localized using a $\langle r^2 \rangle$ minimization procedure prior to the correlation treatment.[54] The STOCKHOLM set of programs[55] were used for the CI calculations.

Some tests of the influence of adding scalar relativistic corrections were made. The corrections were obtained using first-order perturbation theory, including the mass-velocity and Darwin terms,[56,57] and were based on the MCPF density. However, the scalar relativistic effects were found to change the relative energies by at most 0.3−0.5 kcal/mol and were therefore not included in the present paper.

Siegbahn *et al.*[58] recently pointed out that, using well-balanced basis sets of the double-ζ plus polarization type and a correlation treatment at the present level of sophistication, about 80% of the correlation effects on bond energies are normally obtained. Similar estimates of the total correlation effects have been obtained earlier by others, see *e.g.* Gordon and Truhlar.[59] An improved estimate of the relative energies is thus obtained by simply adding 25% of the calculated correlation energy to the MCPF energy. This amounts to adding 20% of the difference between the SCF energy and the total extrapolated energy. The strategy is referred to as the parameterized CI-80 (PCI-80) method[58] and has been adopted in the energy evaluations in the present work.

## 3. Results and Discussion

In the first subsection below, stationary points of ethylene insertion for the present Cr(III) model and their relative energies will be presented and discussed. Whenever possible, geometrical parameters and energies are compared to values reported for a corresponding

(41) Almlöf, J.; Taylor, P. R. *J. Chem. Phys.* **1987**, *86*, 4070.
(42) Raffenetti, R. C. *J. Chem. Phys.* **1973**, *58*, 4452.
(43) Van Duijneveldt, F. B. Research Report No. RJ945, IBM: 1971.
(44) Pou-Amérigo, R.; Merchán, M.; Nebot-Gil, I.; Widmark, P.-O.; Roos, B. O. *Theor. Chim. Acta* **1995**, *92*, 149.
(45) McLean, A. D.; Chandler, G. S. *J. Chem. Phys.* **1980**, *72*, 5639.
(46) Dunning, T. H. *J. Chem. Phys.* **1971**, *55*, 716.
(47) Vosko, S. H.; Wilk, L.; Nusair, M. *Can. J. Phys.* **1980**, *58*, 1200.
(48) Becke, A. D. *Phys. Rev. A* **1988**, *38*, 3098.
(49) Perdew, J. P.; Wang, Y. *Phys. Rev. B* **1992**, *45*, 13244.
(50) Frisch, M. J.; Trucks, G. W.; Schlegel, H. B.; Gill, P. M. W.; Johnson, B. G.; Robb, M. A.; Cheeseman, J. R.; Keith, T.; Petersson, G. A.; Montgomery, J. A.; Raghavachari, K.; Al-Laham, M. A.; Zakrzewski, V. G.; Ortiz, J. V.; Foresman, J. B.; Peng, C. Y.; Ayala, P. Y.; Chen, W.; Wong, M. W.; Andres, J. L.; Replogle, E. S.; Gomperts, R.; Martin, R. L.; Fox, D. J.; Binkley, J. S.; Defrees, D. J.; Baker, J.; Stewart, J. P.; Head-Gordon, M.; Gonzalez, C.; Pople, J. A. *Gaussian 94*; Gaussian, Inc.: Pittsburgh, PA, 1995.
(51) Becke, A. D. *J. Chem. Phys.* **1993**, *98*, 5648.
(52) Lee, C.; Yang, W.; Parr, R. G. *Phys. Rev. B* **1988**, *37*, 785.
(53) Møller, C.; Plesset, M. S. *Phys. Rev.* **1934**, *46*, 618.
(54) Pettersson, L. G. M.; Åkeby, H. *J. Chem. Phys.* **1991**, *94*, 2968.
(55) STOCKHOLM is a general purpose quantum chemical set of programs written by P. E. M. Siegbahn, M. R. A. Blomberg, L. G. M. Pettersson, B. O. Roos, and J. Almlöf. Contact Professor Per E. M. Siegbahn, Department of Physics, University of Stockholm, Sweden, for more information.
(56) Martin, R. L. *J. Chem. Phys.* **1983**, *87*, 750.
(57) Cowan, R. D.; Griffin, D. C. *J. Opt. Soc. Am.* **1976**, *66*, 1010.
(58) Siegbahn, P. E. M.; Blomberg, M. R. A.; Svensson, M. *Chem. Phys. Lett.* **1994**, *223*, 35.
(59) Gordon, M. S.; Truhlar, D. G. *J. Am. Chem. Soc.* **1986**, *108*, 5412.

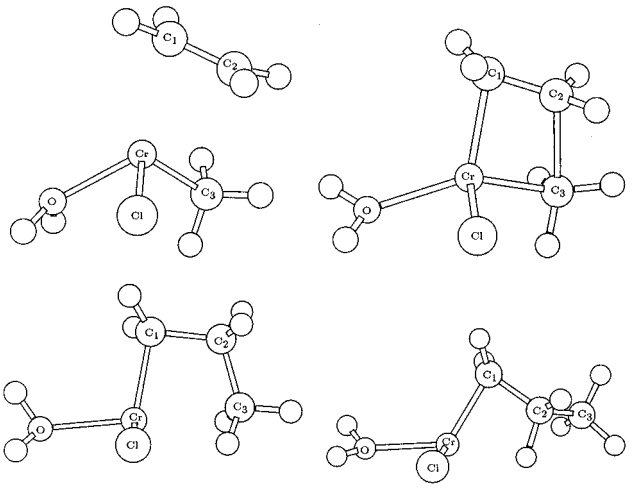

**Figure 1.** Stationary points of ethylene insertion into the Cr−C bond in $CrCl(H_2O)CH_3^+$ as optimized at the BPW91/B level: The $\pi$-complex (upper left), the transition state (upper right), the $\gamma$-agostic product (bottom left), and the $\beta$-agostic product (bottom right). The LSDA-optimized geometries are qualitatively similar to the ones shown above, while at the HF level a different geometrical configuration was found to be the most stable for the TS and the two products of ethylene insertion. In these structures, chlorine is essentially located in the reaction plane, whereas water is oriented essentially perpendicular to this plane.



Ti(IV) model. Both geometrical parameters and energies are reported mainly in terms of gradient-corrected DFT values (BPW91).

The present catalytic system contains a first-row transition metal with a considerable amount of d electrons. In addition, there seems to be little experience with the quantum chemical description of olefin insertion involving chromium as the active metal. Therefore, to ensure acceptable accuracy and to gain experience with this kind of system, a series of methods has been employed in the calculations. Discussion of the accuracy and comparison of the methods are given in the second subsection below.

Where appropriate, the results of the current calculations are compared to experiments involving chromium(III)-based homogeneous catalysts, found in the third subsection below.

**3.1. Main Results for the Insertion Reaction.** Five stationary points of the potential energy surface associated with ethylene insertion were located, namely, the separated reactants $CrCl(H_2O)CH_3^+$ and $C_2H_4$, the $\pi$ complex, the transition state, and two conformers, $\gamma$- and $\beta$-H agostic, of the product. The latter four structures are shown in Figure 1, and important geometrical parameters are given in Table 2. It is immediately clear that the located stationary points are those expected for the well-known Cossee mechanism[60] for ethylene insertion. Thus, the overall picture of the reaction, as emerging from the present geometries, bears considerable resemblance to the results for models of Ti(IV)- and Zr(IV)-based catalysts. This is also true for the important orbital interactions occurring during the reaction, in spite of the fact that group 4 and 6 metals have different electronic structures, as do Ti(IV) and Cr(III) metal ions. This comes about as the three unpaired electrons in our Cr(III) system are all located in the d-orbitals on the metal and do not participate in the bond-forming and breaking.

(60) Cossee, P. *J. Catal.* **1964**, *3*, 80.

**Table 2. Selected Geometrical Parameters at the Stationary Points of Ethylene Insertion in $CrCl(H_2O)CH_3^+$, As Calculated at the BPW91/B Level[a]**

| parameter | reactants | $\pi$ complex | transition state | $\gamma$-agostic product | $\beta$-agostic product |
|---|---|---|---|---|---|
| $r(CrC_1)$ | | 2.25 | 2.06 | 1.98 | 1.97 |
| $r(CrC_2)$ | | 2.44 | 2.31 | 2.57 | 2.34 |
| $r(CrC_3)$ | 1.97 | 1.99 | 2.06 | 2.38 | 3.50 |
| $r(C_1C_2)$ | 1.35 | 1.38 | 1.43 | 1.53 | 1.52 |
| $r(C_2C_3)$ | | 3.22 | 2.21 | 1.57 | 1.54 |
| $r$(CrCl) | 2.12 | 2.16 | 2.18 | 2.17 | 2.16 |
| $r$(CrO) | 2.00 | 2.07 | 2.08 | 2.03 | 2.04 |
| $r(CrH_{agostic})$ | 2.46 | 2.50 | 2.20 | 2.05 | 1.90 |
| $r(CH_{agostic})$ | 1.11 | 1.11 | 1.12 | 1.13 | 1.17 |
| $\angle C_1CrC_3$ | | 110.9 | 96.4 | 71.3 | 47.4 |
| $\angle C_1CrO$ | | 132.1 | 118.0 | 103.6 | 120.2 |
| $\angle C_3CrO$ | 113.3 | 96.6 | 136.3 | 159.0 | 148.1 |
| $\angle C_1CrCl$ | | 108.7 | 102.9 | 112.7 | 111.9 |
| $\angle C_3CrCl$ | 111.6 | 113.5 | 108.1 | 105.7 | 117.8 |
| $\angle ClCrO$ | 122.8 | 93.9 | 90.6 | 95.1 | 94.0 |
| $\angle CrC_3H_{agostic}$ | 102.6 | 103.6 | 81.9 | 58.9 | |
| $\angle CrC_1C_2$ | | 80.8 | 80.5 | 93.1 | 83.2 |
| $\angle C_1C_2C_3$ | | 89.5 | 113.7 | 111.5 | 116.8 |
| $\angle C_2C_1CrC_3$ | | −61.4 | −16.2 | −15.4 | −27.8 |
| $\angle C_1CrC_3H_{agostic}$ | | −55.9 | 157.0 | 145.5 | |
| $\angle HOCrH_{water}$ | 152.3 | 136.5 | 148.8 | 129.4 | 141.5 |

[a] In Angstroms and degrees. The nonagostic C−H bonds make a narrow spread about 1.10 Å. Likewise, the mean of the two $r$(OH) values is 0.98 Å throughout.

The important orbital interactions follow the pattern described for ethylene insertion in $TiCl_2CH_3^+$.[18] In the reactant, the highest doubly occupied molecular orbital (MO) is the Cr−methyl $\sigma$ orbital. The second lowest unoccupied orbital has a high degree of d-character and is seen to be a suitable $\sigma$-acceptor orbital with a large lobe at the vacant site. In the $\pi$ complex, this orbital mixes with the ethylene $\pi$ orbital to form a donor−acceptor $\sigma$-bonding orbital between ethylene and the metal. At the transition state (TS), where the metal has to maintain bonds to both the methyl (polymer chain) and the inserting ethylene, this is achieved through two MOs which carry large components from the original Cr−methyl and Cr−ethylene $\sigma$-bonding orbitals. At the TS, the orbital dominated by the chromium−methyl $\sigma$ bond mixes with the ethylene $\pi^*$ orbital for the metal to also obtain a $\sigma$-bonding interaction with the closest carbon of ethylene. The initial, weak bonding between ethylene and the methyl group is accounted for by the MO dominated by the Cr−ethylene donor−acceptor orbital from the $\pi$ complex.

**3.1.1. The $CrCl(H_2O)CH_3^+$ and $C_2H_4$ Reactants.** The $CrCl(H_2O)CH_3^+$ reactant (not shown, but qualitatively similar to the chromium fragment of the $\pi$ complex, cf. upper left structure of Figure 1) has a slightly bent, pyramidal structure. The methyl group nearly displays local $C_{3v}$ symmetry, with HCH angles between 109.9 and 111.6°. However, one of the C−H bonds is slightly longer than the other two and has a CrCH angle of 102.6°, indicating a weak agostic interaction. This interaction seems to be of approximately the same order as that found in $TiCl_2CH_3^+$ at the correlated level,[22] but definitely weaker than what has been calculated for the corresponding titanocene and zirconocene catalysts.[22−24,27−29,31]

The three unpaired electrons are located in metal-centered orbitals of d character, one of which is an out-of-plane $t_{2g}$-like orbital. The other two are $e_g$-like out-of-plane orbitals. Two of these half-filled orbitals are weakly polarized with the largest lobes pointing toward the empty site, which are thus probably responsible for the slightly bent, pyramidal structure.

The highest doubly occupied molecular orbital (MO) in the reactant is the Cr−methyl $\sigma$ orbital. In standard *ab initio* treatments of correlation effects, like MP2 and SDCI, the most important excited configuration by far is the Cr−methyl antibonding, $\sigma^2 \rightarrow \sigma^{*2}$. The analogous excitation has been described for Ti(IV) systems[22,61] and is the reason why spin-restricted solutions for these systems are found to possess instability toward becoming unrestricted.[18,22,61] Indeed, such an instability was also detected for the present chromium system. A covalent chromium−methyl bond could, however, not be obtained at the unrestricted HF level, implying that a lifting of the spin symmetry is not enough for describing this correlation effect properly. Inclusion of a dynamical correlation corrects the deficiency. Spin-unrestricted DFT calculations predict the existence of a covalent bond, as do standard correlated methods which include double excitations from the zero-order restricted HF wave function.

The metal to chlorine bond consists, as expected, of a Cr−Cl $\sigma$-bonding orbital, polarized toward Cl, as well as two $\pi$ bonding MOs accounting for the $\pi$ donating abilities of chlorine. Thus, the MOs involved in the metal−chlorine bond are similar to the orbitals involved in metal−cyclopentadienyl bonds, which of course is essential to justify the use of chlorine as a model of the electronic effects associated with Cp. The model can be characterized as having an isolobal relationship to the real catalyst system, $CrCp^*(THF)CH_3^+$. The reaction profile obtained with this model is not, of course, quantitatively correct, but the relationship to the real catalytic system should be close enough to afford qualitative insight into the function of the latter.

Water acts as a donor in this complex and constitutes a labile ligand which is relatively easily moved around in the coordination sphere. In the present calculations, water is used as a model of tetrahydrofuran (THF). A comparison between the metal−donor bonds involving water, dimethyl ether (DME), and THF as the donor is made in a later subsection.

**3.1.2. The $\pi$ Complex.** Upon coordination of ethylene, the pyramidal structure becomes more pronounced and the relatively weakly bound water ligand bends down to make room for incoming ethylene. Looking down the Cr−ethylene axis in the most stable conformer of the $\pi$ complex, ethylene is oriented parallel to the chromium−oxygen bond. The $\pi$ complex itself is perhaps best approximated by a tetrahedral configuration with $C_1$ as the fourth ligand coordinated to chromium. The entering of the ethylene molecule into the coordination sphere of the metal only imposes relatively small changes to the other bond distances in the complex, typically increasing them by a few hundredths of an Angstrom. The largest change occurs for the metal−water donor−acceptor bond, which is lengthened from 2.00 to 2.07 Å. The already weak α-H agostic interaction is left almost unchanged upon coordination, and thus, the $\pi$ complex also offers an almost undistorted methyl group.

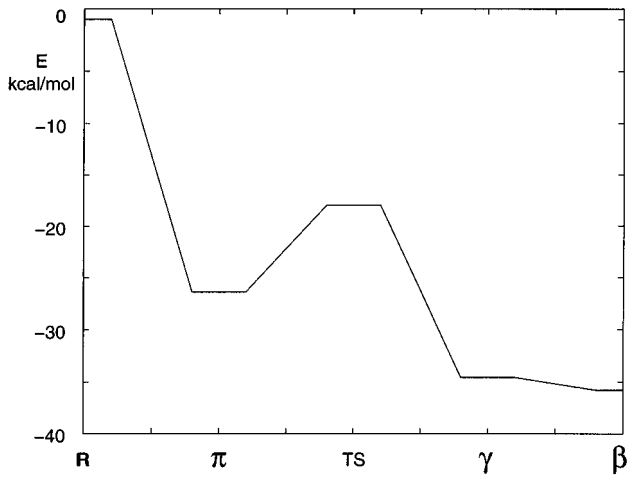


**Figure 2.** BPW91/C energy profile for ethylene insertion into the Cr−C bond in $CrCl(H_2O)CH_3^+$. The symbols below the abscissa designate: R, separated reactants; $\pi$, $\pi$ complex; TS, transition state of insertion; $\gamma$, $\gamma$-agostic product; and $\beta$, $\beta$-agostic product.

**Table 3. Comparison of Energies (kcal/mol) of Ethylene Insertion[a]**

| method[a] | $D_e(\pi)$ | $E_{act}$ | $-E_{rxn}$ |
|---|---|---|---|
| | $CrCl(H_2O)CH_3^+$ [b] | | |
| HF/B | 22.3 | 20.7 | 26.4 |
| MP2/C | 28.7 | 9.0 | 41.0 |
| PCI-80/A | 28.0 | 10.2 | 39.5 |
| | $TiCl_2CH_3^+$ [c] | | |
| HF | 35.2 | 12.3 | 40.8 |
| MP2 | 42.0 | 2.6 | 57.9 |
| CCSD(T) | 38.7 | 5.2 | 51.2 |

[a] $D_e$ ($\pi$) is the $\pi$ complexation energy, $E_{act}$ is the activation energy relative to the $\pi$ complex, and $-E_{rxn}$ is the exothermicity from the separated reactants to the $\gamma$-agostic product. [b] HF/B means HF with basis B as described in the Computational Details section. The HF/B results were obtained for geometries optimized at that level. The MP2/C and PCI-80/A energies were obtained for geometries optimized at the BPW91/B level. [c] Energies, calculated using restricted determinant wave functions, taken from ref 22, and based on MP2 optimized geometries. The basis sets were [5s3p2d] for Ti, split-valence (SV) plus polarization for C and Cl, and SV for H.

The calculated BPW91/C energy profile of ethylene insertion is shown in Figure 2. In Table 3, the HF, MP2, and CI results for the present system are compared to the corresponding results for the $TiCl_2CH_3^+$ model reported by Weiss *et al.*[22] It is evident that complexation of ethylene is about 10 kcal/mol weaker for our chromium(III) model than for $TiCl_2CH_3^+$, probably as a result of the increased repulsion due to the unpaired electrons present in the former. A closer look at the half-filled orbitals shows that there is an interaction, although very weak, between the metal d and ethylene $\pi^*$ MOs contributing to the metal−ethylene bond. Back-donation to ethylene is generally not observed for the group 4 $d^0$ model catalysts.[18,27,62,63]

**3.1.3. Transition State of Insertion.** The essential part of the located TS of insertion (cf. upper right

(61) Weiss, H.; Haase, F.; Ahlrichs, R. *Chem. Phys. Lett.* **1992**, *194*, 492.

(62) Jensen, V. R.; Ystenes, M.; Wärnmark, K.; Åkermark, B.; Svensson, M.; Siegbahn, P. E. M.; Blomberg, M. R. A. *Organometallics* **1994**, *13*, 282.

(63) Jensen, V. R.; Børve, K. J.; Westberg, N.; Ystenes, M. *Organometallics* **1995**, *14*, 4349.

**Table 4. Comparison of Important Bond Distances (Å) at the Transition State and Products of Ethylene Insertion[a]**

| | transition state | | | $r(CH_{agostic}) - r(CH)$[b] | |
|---|---|---|---|---|---|
| | $r(MC_3) - r(MC_1)$ | $r(C_1C_2)$ | $r(C_2C_3)$ | $\gamma$-agostic product | $\beta$-agostic product |
| | | | $CrCl(H_2O)CH_3^+$ | | |
| HF | 0.08 | 1.42 | 2.17 | 0.03 | 0.06 |
| LSDA | −0.07 | 1.41 | 2.27 | 0.03 | 0.07 |
| BPW91 | 0.00 | 1.43 | 2.21 | 0.03 | 0.07 |
| | | | $TiCl_2CH_3^+$ | | |
| HF[c] | −0.03 | 1.41 | 2.17 | 0.03 | 0.07 |
| MP2[d] | −0.19 | 1.39 | 2.39 | 0.02 | |

[a] $C_3$ is the carbon bound to the metal in the reactant, while $C_1$ is bound to the metal in the product. [b] $r$(CH) designates the mean of the nonagostic C−H distances (1.10 Å). [c] Structures 3a, 4a, and 4e from ref 18. The basis sets were [5s3p2d] for Ti and 3-21G for the rest of the elements. The $C-H_{methylene}$ distances were not given, so the $C-H_{methyl}$ distance (1.08 Å) was used instead. [d] From ref 22. The basis sets were [5s3p2d] for Ti, SV plus polarization for C and Cl, and SV for H.

**Table 5. Mulliken Populations and Charges ($e$) for the Reactants, the $\pi$ Complex, the Transition State, and the Products of Ethylene Insertion[a]**

| | reactants | $\pi$ complex | TS of insertion | $\gamma$-agostic product | $\beta$-agostic product |
|---|---|---|---|---|---|
| | | | Cr populations | | |
| 3d | 4.49 | 4.57 | 4.61 | 4.63 | 4.61 |
| 4s | 0.34 | 0.33 | 0.28 | 0.31 | 0.30 |
| 4p | 0.30 | 0.40 | 0.44 | 0.39 | 0.38 |
| | | | Charges | | |
| Cr | 0.85 | 0.68 | 0.65 | 0.66 | 0.70 |
| $C_1$ | −0.28 | −0.33 | −0.39 | −0.47 | −0.47 |
| $C_2$ | −0.28 | −0.25 | −0.28 | −0.25 | −0.21 |
| $C_3$ | −0.67 | −0.66 | −0.61 | −0.52 | −0.48 |
| $H_2O$ | 0.24 | 0.23 | 0.20 | 0.25 | 0.22 |
| Cl | −0.08 | −0.14 | −0.16 | −0.14 | −0.14 |

[a] The populations were calculated at the BPW91/C level.

structure of Figure 1) has a four-center ring structure consisting of ethylene, the methyl group, and chromium, consistent with Cossee's proposal[60] for Ziegler−Natta polymerization catalysts. Four-center transition states of this kind have also been located in a number of quantum chemical studies of group 4 polymerization catalysts, see *e.g.* refs 17, 18, 24, and 26. The "active" part of the structure (the ring) is almost planar, with the weakly bound water molecule being essentially in-plane and positioned opposite to the active bonds, Cr−$C_1$ and Cr−$C_3$. Chlorine on the other hand, is almost perpendicular to the plane of reaction.

The present transition state of insertion is located in the middle of the insertion, as judged from the forming and breaking Cr−C bonds being equal and with a relatively long ethylenic C−C bond (1.43 Å). This TS seems to be somewhat late compared to what is typically found for $TiCl_2CH_3^+$;[18,22] see also Table 4.

The stabilizing effect of an agostic interaction on the TS has been noted in several theoretical works on group 4 catalysts, see *e.g.* refs 18, 24, 26, and 28, and is also supported by experimental efforts.[64] A relatively strong agostic interaction is also seen in the present TS, the CrCH angle being much sharper (81.9°) than that in the $\pi$ complex (103.6°) and with the agostic C−H bond being two hundredths of an Angstrom longer than the other C−H distances. In fact, the interaction seems to be of approximately the same strength as that for $TiCl_2CH_3^+$, the lengthening of the $C-H_{agostic}$ bond compared to the other C−H bonds being roughly the same for the two models (cf. Table 4).

The energy profile of insertion in Figure 2 shows evidence of a feasible reaction with a low (8.4 kcal/mol) activation energy. Comparing the calculated activation energies for the chromium(III) and titanium(IV) system in Table 3, it seems, however, that the latter are uniformly lower, the difference being 5 kcal/mol when comparing the CI results. We cannot, at the present stage, conclude that this reflects a difference between the two corresponding real catalysts but there are observations indicating that this is the fact. Only minor differences are noticed when improving the present model by replacing Cl by Cp.[65] In fact, Cp increases the barrier slightly, while introducing Cp to the Ti(IV) model is known to reduce or remove the barrier of insertion,[22] thus suggesting that the difference between the real catalysts should be even more pronounced.

Among the well-known features of olefin insertion reactions reported for group 4 catalysts is the reduced positive charge on the metal in the transition state region,[26,66−68] mostly as a result of the higher d population. The reason is that the metal connects the polymer chain and the monomer, if possible, through d-rich bonds at the transition state. Another reason for increasing the d population at the TS is that the metal may polarize away s electrons that are repulsive against the olefin, thus reducing the barrier significantly.[66,67] An increase in the d population at the TS is also found for the present system (cf. Table 5), but it is rather small, and also present in the products. This indicates that the present increase in the d population may simply be a result of the growing size of the cation during the reaction rather than the importance of the d orbitals at the TS. In fact, less utilization of the d orbitals could be expected for chromium(III), as essentially all of the d orbitals are occupied already in the reactant, leaving the metal with relatively little freedom to use them in forming new hybrid orbitals. The same effect has been noted earlier for ethylene insertion using molybdenum-based models.[66] However, as a result of the positive charge on the present system, the amount of repulsive s electrons is relatively small and the barrier to insertion rather low, within the range (6−12 kcal/mol) reported for Ziegler−Natta catalysts.[69−72] To conclude, the higher barrier to insertion found for the present system compared to $TiCl_2CH_3^+$ seems to be caused partly by the decreased possibility of using the d orbitals in hybridization and partly by the increased repulsion against the olefin resulting from the nonbonding d electrons on the metal.

**3.1.4. The $\gamma$- and $\beta$-Agostic Products.** Both of the optimized product geometries (the two lower structures of Figure 1) bear a resemblance to the reactant, with

(64) Piers, W. E.; Bercaw, J. E. *J. Am. Chem. Soc.* **1990**, *112*, 9406.
(65) Jensen, V. R.; Børve, K. J. Manuscript in preparation.
(66) Siegbahn, P. E. M. *Chem. Phys. Lett.* **1993**, *205*, 290.
(67) Jensen, V. R.; Siegbahn, P. E. M. *Chem. Phys. Lett.* **1993**, *212*, 353.
(68) Alsberg, B. K.; Jensen, V. R.; Børve, K. J. *J. Comput. Chem.* **1996**, *17*, 1197.
(69) Natta, G.; Pasquon, I. *Adv. Catal.* **1959**, *11*, 1.
(70) Machon, J.; Hermant, R.; Hoteaux, J. P. *J. Polym. Sci. Symp.* **1975**, *52*, 107.
(71) Chien, J. C. W. *J. Am. Chem. Soc.* **1959**, *81*, 86.
(72) Chien, J. C. W.; Razavi, A. *J. Polym. Sci., Part A: Polym. Chem.* **1988**, *26*, 2369.

the alkyl, chlorine, and water ligands occupying a pyramidal arrangement around chromium. However, the similarities to the $\pi$ complex are perhaps more obvious, the ligand−metal−ligand angles being consistent with a pyramidal structure that is more bent than in the reactant. The reason for this bending is an agostic interaction, which in both product structures is far stronger than in the reactant, and the hydrogen involved acts in some respects as a fourth ligand in the complex.

The product structures obtained for the present system have much in common with the products of an ethylene insertion for group 4 metals. Kawamura-Kuribayashi *et al.*[18] located the $\gamma$- and $\beta$-agostic products of ethylene insertion in $TiCl_2CH_3^+$ at the HF level, while Weiss *et al.*[22] only obtained the $\gamma$-agostic conformation at the MP2 level. For the present system, no α-agostic product structure could be obtained regardless of the level of geometry optimization. The reason for this is the low degree of steric hindrance resulting from the small model ligands. An α-agostic arrangement of the propyl group immediately rotates to give the energetically preferred structure with the strongest agostic interaction, the $\beta$-conformation (lower right structure of Figure 1). It is reasonable to believe that sterically more demanding ligands, such as Cp* and THF, may stabilize the α-conformation, as is the case when replacing the chlorines with Cp in $TiCl_2CH_3^+$.[22] Furthermore, the similarities between the current Cr(III) system and $TiCl_2CH_3^+$ are also striking when investigating the details of the product structures. The agostic interactions in the two product conformations seem to be of approximately the same strength, as calculated for the corresponding titanium sytem (cf. Table 4), again the lengthening of the agostic C−H bonds are found to be very similar.

It appears that the overall exothermicity for insertion to give the kinetic $\gamma$-agostic product is considerably smaller than the one calculated for the titanium(IV) analogue (cf. Table 3). Some of this difference, however, can probably be attributed to the smaller basis sets used in the calculations on the Ti(IV) model, with a larger expected basis set superposition error (BSSE) than in the present calculations. In addition, the interaction between the propyl group and the metal in the product makes it exceedingly difficult to estimate a correct value for the overall insertion energy from simple gas-phase reactions. Much of the difference between Ti and Cr in the interaction with the propyl group can simply be ascribed to the difference in the acidity of the metals. The difference in acidity can, however, be found already in the $\pi$-coordination step. Very similar results should, therefore, be expected for the two metals for the liberation of energy when going from the $\pi$ complex to the product. This is seen to be the case; the exothermicities obtained at the two highest highest levels (PCI-80 and CCSD(T)) were 11.5 and 12.5 kcal/mol for the chromium and titanium model, respectively.

Our finding that the $\beta$-agostic conformation is the more stable conformation (by about 1 kcal/mol) is in line with the relative stabilities calculated at the correlated level between $\gamma$- and $\beta$-agostic propyl structures of group 4 metallocene catalysts, see *e.g.* refs 22 and 24. There has been an increasing interest in the possible role of the different agostic orientations of the polymer chain in the catalyst.[22,24,28,29,31] This is perhaps best illustrated by the fact that Lohrenz *et al.*,[29] relying on DFT results on ethylene insertion in $ZrCpC_2H_5^+$, recently claimed that the propagation barrier itself is due to a reorientation between agostic conformations of the polymer chain. The study of the rotational barriers between the agostic structures is not relevant for the present system due to the small model ligands.

**3.2. Comparison of Methods. 3.2.1. Methods for Geometry Optimization.** The difference in length between the forming and breaking Cr−methyl bonds, $r(MC_3) - r(MC_1)$, given in Table 4, may be used to classify the TS of insertion. The HF-optimized TS is seen to be located late during insertion, with the breaking metal−carbon bond being longer than the one being formed. BPW91 provides a TS belonging right in the middle of the reaction and as such appears to represent a balanced description of the system in the transition region. Inclusion of excess correlation, as in LSDA, leads to a TS located early during insertion. A short ethylenic C−C bond and a long forming C−C bond are also seen to be characteristics of an early transition state. At this point, it should be noted that at the HF level, a different geometrical configuration was found to be the most stable for the TS and the products. HF appeared to stabilize structures where Cl and $H_2O$ have their positions interchanged compared to the BPW91-optimized structures given in Figure 1. The energy difference between these two configurations is small, −0.5 kcal/mol at the HF/B level and +2.1 calculated with BPW91/B for the $\gamma$-agostic product.

Among the geometry parameters of particular interest, it can be noticed that the lengthening of the C−H bonds as a result of an agostic interaction varies little with the method of optimization (cf. Table 4). The choice of method for optimization does, however, influence the corresponding chromium−hydrogen bond lengths. The $Cr-H_{agostic}$ distances for the $\beta$-agostic structure were 2.01, 1.82, and 1.90 Å for HF, LSDA, and BPW91, respectively. These results indicate that the potential for the $Cr-H_{agostic}$ stretch is flat in the region around the minimum and that the description of the agostic interaction may still be intact, even with a seemingly long metal−hydrogen distance, as for HF. In fact, relatively little influence was found from the level of geometry optimization in the description of such weak interactions in titanium−propyl complexes.[73]

**3.2.2. Methods for Obtaining Energies.** Energies are given relative to the separated reactants, Table 6. Excluding HF and LSDA, the differences between the methods are surprisingly small and most of the variance is readily explained. Both the ethylene binding energies and activation energies follow the expected pattern that correlation effects stabilize structures where more electrons are gathered. HF does not include electron correlation, while LSDA overestimates the correlation energy.[74] In line with this, HF and LSDA define the extremes among the estimates of the ethylene binding energy and the activation energy. MP2 is also known to exaggerate correlation effects and provides a high estimate of the ethylene binding energy as well as a low value for $E_{act}$. Among the estimates of the ethylene

(73) Jensen, V. R.; Børve, K. J. Manuscript in preparation.
(74) Parr, R. G.; Yang, W. *Density-Functional Theory of Atoms and Molecules*; Oxford University Press: Oxford, 1989; p 180.

**Table 6. Energies (kcal/mol) of Ethylene Insertion for $CrCl(H_2O)CH_3^+$ [a]**

| method[b] | $\pi$ complex | TS of insertion | $\gamma$-agostic product | $\beta$-agostic product | $E_{act}$ |
|---|---|---|---|---|---|
| LSDA/B | −41.2 | −37.5 | −55.9 | −54.6 | 3.7 |
| BPW91/B, C | −26.6, −26.4 | −18.3, −18.0 | −34.6, −34.6 | −35.7, −35.8 | 8.4, 8.4 |
| B3LYP/C, D | −24.6, −23.1 | −13.6, −11.3 | −33.1, −30.0 | −33.9, −31.0 | 11.1, 11.8 |
| HF/B, C | −22.3, −20.1 | −1.6, −1.6 | −26.4, −26.4 | −27.7, −27.7 | 20.7, 20.4 |
| MP2/C | −28.7 | −19.7 | −41.0 | −42.0 | 9.0 |
| MCPF/A | −26.7 | −14.6 | −37.5 | −38.5 | 12.1 |
| PCI-80/A | −28.0 | −17.8 | −39.5 | −40.8 | 10.2 |

[a] The activation energy ($E_{act}$) is given relative to the $\pi$ complex. All other energies are given relative to separated reactants. [b] LSDA/B means LSDA with basis B as described in the Computational Details section. The LSDA/B and HF/B results were obtained for geometries optimized at those levels. All the other energies were obtained for geometries optimized at the BPW91/B level.

binding energies, PCI-80, MCPF, and BPW91 follow close below the estimate by MP2. B3LYP predicts a binding energy intermediate between that of HF and the other correlated methods (excluding LSDA), suggesting that the hybrid B3LYP includes less correlation energy than pure DFT, represented by BPW91, and standard correlated methods like MP2. There is a remarkable agreement between the scaled MCPF (PCI-80) result, MP2, and BPW91 for the activation energy, with estimates within an interval of 2 kcal/mol. B3LYP is also close to this group and only about 1 kcal/mol higher than PCI-80, but apparently it once more includes less correlation than pure DFT and our best *ab initio* estimate. It is somewhat surprising that the computationally cheap MP2 method is able to provide relative energies for reactions involving transition metals comparable to those obtained from more sophisticated CI methods. The reason is probably absence of severe near degeneracy in the present chemical system.

Somewhat larger differences among the methods can be noticed for the overall exothermicity of the insertion. Limiting the comparison to the exothermicity upon going from the $\pi$ complex to the products, the differences are significantly reduced and the resolution enhanced. The exothermicities from the $\pi$ complex to the primary $\gamma$-agostic product were 8.2, 8.5, 12.3, 10.8, and 11.5 kcal/mol for BPW91/C, B3LYP/C, MP2/C, MCPF/A, and PCI-80/A, respectively. Some of the differences in the predicted exothermicity can be explained by their corresponding performance on the simple gas-phase reaction $CH_3 + C_2H_4 \rightarrow C_3H_7$, which were 27.6, 26.6, 29.0, 27.2, and 28.0 kcal/mol for the methods listed above, respectively. It is evident that the trend in exothermicity from the simple gas-phase reaction is found in the exothermicity for the catalytic reaction with one exception BPW91. The pure DFT method predicts a relatively high exothermicity for the radical reaction but is still the lowest for the catalytic one. It, thus, seems as though DFT predicts less relative stability than correlated *ab initio* methods do for the present agostic product structures. At this point, it should, however, be borne in mind that the variance between the methods in predicting the exothermicity is small.

**3.2.3. Basis Set Effects.** Extending set C, with diffuse functions on the ligands as well as double polarization, introduces significant but readily explainable changes to the B3LYP relative energies. The effect is most easily seen in the calculated overall exothermicity, where a basis set effect of about 3 kcal/mol can be noticed upon improving from basis C to D. A basis set effect of this magnitude is expected when breaking the ethylene $\pi$ bond[75] and will show up in the overall exothermicity of an ethylene insertion process if not masked by large interactions with the product chain.[73] This effect originates from the fact that alkenes and alkanes are not equally far from the HF limit at a given level of basis set.[73,75] For reactions involving breaking of the ethylene $\pi$ bond, it is thus possible to restrict the basis sets to being of double-$\zeta$ plus polarization quality by adding a correction for failure to approach the HF limit. For the overall reaction energy, this correction is about 3 kcal/mol. For the intermediate structures, such as the TS, a semi-empirical relationship[76] between bond order and bond length can be used. Here, as much as half of the effect for the overall reaction comes into play in the $\pi$-coordination step, which indicates that a significant portion of the $\pi$ bond in ethylene is broken already at this point. This also indicates that the BSSE involved in the coordination step is rather small for our B and C sets.

Extending B with one f function on chromium and a p on hydrogen to become the C set only introduces minor changes to the BPW91 energies. The difference between our HF ethylene binding energies with the B and C sets may seem large, but this difference includes the effect of changing from HF-optimized to BPW91-optimized geometries.

**3.3. Comparison with Experiment.** Theopold *et al.*[8] reported the crystal structure of $[CrCp^*(THF)_2CH_3]^+BPh_4^-$. In the present cation, $CrCl(H_2O)CH_3^+$, Cp* and THF are modeled by chlorine and water, respectively. Direct comparison with the reported crystal structure is thus difficult, and perhaps the Cr−O and Cr−methyl bonds are the most relevant. Our values for these distances (cf. Table 2) are seen to be significantly shorter than those reported (2.042 and 2.056 Å, respectively). Adding a second water molecule to model the di-THF compound makes the distances, now 2.01 and 2.10 Å for Cr−O and 2.00 Å for Cr−methyl, come out in somewhat better agreement with the X-ray diffraction data by Theopold *et al.*

Since water is used as a model for THF, a comparison of the metal−donor bond between water, dimethyl ether (DME), and THF was performed, cf. Table 7. The orbitals (not shown) involved in the metal−donor interaction are rather similar for the three complexes, although the overlap increases with the size of the donor. The two larger donors are also found (cf. Table 7) to have higher Mulliken charges in the complexes, confirming their better donating abilities. This, in turn, contributes to the metal−donor bond strength, the binding energy of water being some 17 kcal/mol lower than that of THF. It is reasonable to believe that a

(75) Børve, K. J.; Jensen, V. R. *J. Chem. Phys.* **1996**, *105*, 6910.

(76) Johnston, H. S. *Gas Phase Reaction Rate Theory*; Ronald Press: New York, 1966.

**Table 7. Bond Energies (kcal/mol) and Mulliken Charges (*e*) on the Donors L for $CrClCH_3^+$−L and $CrClCH_3L^+$−L Complexes[a]**

| L | method[a] | $D_e$-($CrClCH_3^+$−L) | $q_L$ | $D_e$-($CrClCH_3L^+$−L) | $q_L$ |
|---|---|---|---|---|---|
| $H_2O$ | B3LYP/C | 52.1 | 0.22 | 36.8 | 0.17 |
| | B3LYP/D | 46.4 | | 32.3 | |
| DME[b] | B3LYP/C | 59.2 | 0.31 | | |
| | B3LYP/D | 56.0 | | | |
| THF[c] | B3LYP/C | 66.3 | 0.32 | | |
| | B3LYP/D | 63.5 | | | |

[a] All energies were obtained for geometries optimized at the BPW91/B level. [b] Dimethyl ether. [c] Tetrahydrofuran.

somewhat higher Lewis acidity can be expected for the model catalyst with water instead of THF.

From the binding energies of water, DME, and THF in Table 7, it is clear that ethylene should experience difficulties in displacing these donors. Even the binding energy of the second water molecule is some 10 kcal/mol larger than that of ethylene, and it is likely that the difference to the second THF (not calculated) is even larger. This is in agreement with the experimental fact[8,9] that adding THF reduces the polymerization rate.

The energies of the TS relative to the reactants and the $\pi$ complex ($E_{act}$) are given in Table 6. It turns out that, excluding HF and LSDA, the calculations predict activation energies in the range 8−12 kcal/mol, in excellent agreement with the measurement (8 kcal/mol) for the $[CrCp^*(THF)_2CH_3]^+$ $BPh_4^-$ catalyst.[8]

## 4. Conclusions

We have seen that the present chromium(III) system displays many similarities to the corresponding group 4 systems for which several theoretical studies are available. The located stationary points are those expected for the direct insertion mechanism and are very similar to corresponding structures calculated for group 4 systems.

Judging from the equal lengths of the forming and breaking Cr−C bonds, the present transition state is located in the middle of the insertion, which appears to be somewhat later than that found in the corresponding group 4 systems. Furthermore, the insertion reaction using chromium(III) catalysts seems to be feasible, with a low activation energy measured for the real catalyst as well as calculated for the present model. However, the calculated activation energy (8−12 kcal/mol) is still a few kcal/mol higher than that for a titanium(IV)-based model catalyst, which may reflect a difference between the corresponding real catalysts. The higher barrier to insertion for the chromium(III) system can be attributed partly to an increased repulsion to the olefin from the nonbonding d electrons on the metal and partly to a reduced accessibility of d orbitals to participate in hybridization during the reaction. The various methods employed in the present study, ranging from Hartree−Fock through MP2 and size consistent CI to pure and hybrid DFT methods, display less variance than what could be expected for a first-row transition metal system with significant d population. This is encouraging and suggests that larger, realistic systems of this kind may be studied with any of the correlated methods used here (excluding LSDA), together with modest basis sets of double-$\zeta$ plus polarization quality.

**Acknowledgment.** This research was financially supported by The Norwegian Academy of Science and Letters and Den norske stats oljeselskap a.s. (VISTA, Grant No. V6415), and also received a grant of computing time from the The Research Council of Norway (Programme for Supercomputing).

OM960930K